Heliyon 10 (2024) e28159

Contents lists available at ScienceDirect

Heliyon

journal homepage: www.cell.com/heliyon

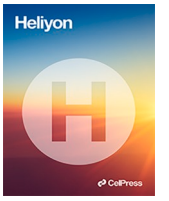

Research article

Characterization of water-soluble ions in PM_{10} over an industrial area in northern Colombia: Temporal variations and correlation with satellite data

Roberto Rojano [a,*], Heli A. Arregocés [a,b], Gloria Restrepo [b]

[a] Grupo de Investigación GISA, Facultad de Ingeniería, Universidad de La Guajira, km 3+354 Vía Riohacha- Maicao, Riohacha, Colombia
[b] Grupo Procesos Fisicoquímicos Aplicados, Facultad de Ingeniería, Universidad de Antioquia SIU/UdeA, Calle 70 No. 52–21, Medellín, Colombia

ARTICLE INFO

Keywords:
PM_{10}
Water-soluble ions
Sulfate-aerosol
Correlation
Marine-aerosols

ABSTRACT

This study was designed to assess the concentrations of nine water-soluble ions in PM_{10} mass at two sites of an open-pit coal mine and to analyze the correlation and variation of the spatial distribution of sulfate ions with the PM_{10} sulfate aerosol optical depth at 550 nm (suaod550) in two (North and South) stations of the study area. The daily average of PM_{10} concentrations ranged from 20.48 to 53.10 $\mu g/m^3$ and thus did not exceed the daily average maximum permissible level of PM_{10} (100 $\mu g/m^3$) established in the Colombia standard at any station. The concentrations of nine water-soluble ions in PM_{10} (Cl^-, NO_3^-, PO_4^{3-}, SO_4^{2-} Na^+, NH_4^+, K^+, Mg^{2+}, and Ca^{2+}) were determined. The ions under analysis, $SO4^{2-}$, Na^+, and NH_4^+ had the highest concentrations. Combined, they accounted for 75% of the mass of water-soluble ions in a total of 210 samples. The SO_4^{2-} concentrations in PM_{10} significantly correlated with suaod550 (r ranging from 0.57 to 0.66), emphasizing the strong effect of suaod550 from Venezuela (Lake Maracaibo) on central and northern Colombia. These results demonstrate that the effects of local sulfate emissions near monitoring sites can be predicted and assessed using satellite data.

1. Introduction

Air pollution kills millions of people annually, decreases the quality of life, and is the main environmental threat to human health [1]. The Environmental Protection Agency (EPA) and the World Health Organization (WHO) consider particulates, also known as particulate matter (PM), as criteria air pollutants with scientific evidence of posing short- and long-term risks to human health [1,2]. The public health impact of PM has been reported in the last decade [3–7]. Its effects on local climate and ecology have also garnered considerable research interest [8–11]. PM has been identified as the main source of air pollution in open-pit mining, especially total suspended particles and particles smaller than 10 μm (PM_{10}) [12–14]. Among the environmental impacts of open-pit coal mines, their impact on air quality is the most controversial and the most systematically monitored.

High PM concentrations have been recorded in communities near mining excavations and are often much higher than those in large urban centers [15]. Reported evidence confirms that interactions with or proximity to mining activity increase morbidity and mortality in these communities [16–24]. Therefore, the chemical compounds in PM mass must also be identified.

The chemical composition of PM emitted from open-pit coal mining operations may be influenced by primary and secondary

* Corresponding author.
E-mail address: rrojano@uniguajira.edu.co (R. Rojano).

https://doi.org/10.1016/j.heliyon.2024.e28159
Received 10 November 2023; Received in revised form 27 February 2024; Accepted 13 March 2024
Available online 15 March 2024

Nomenclature

PM	Particulate matter
PM_{10}	PM less than 10 μm in diameter
AOD	Aerosol optical depth
suaod550	sulfate aerosol optical depth at 550 nm
Open-pit	Surface mining technique
SD	Standard deviation
CAMS	Copernicus Atmosphere Monitoring Service

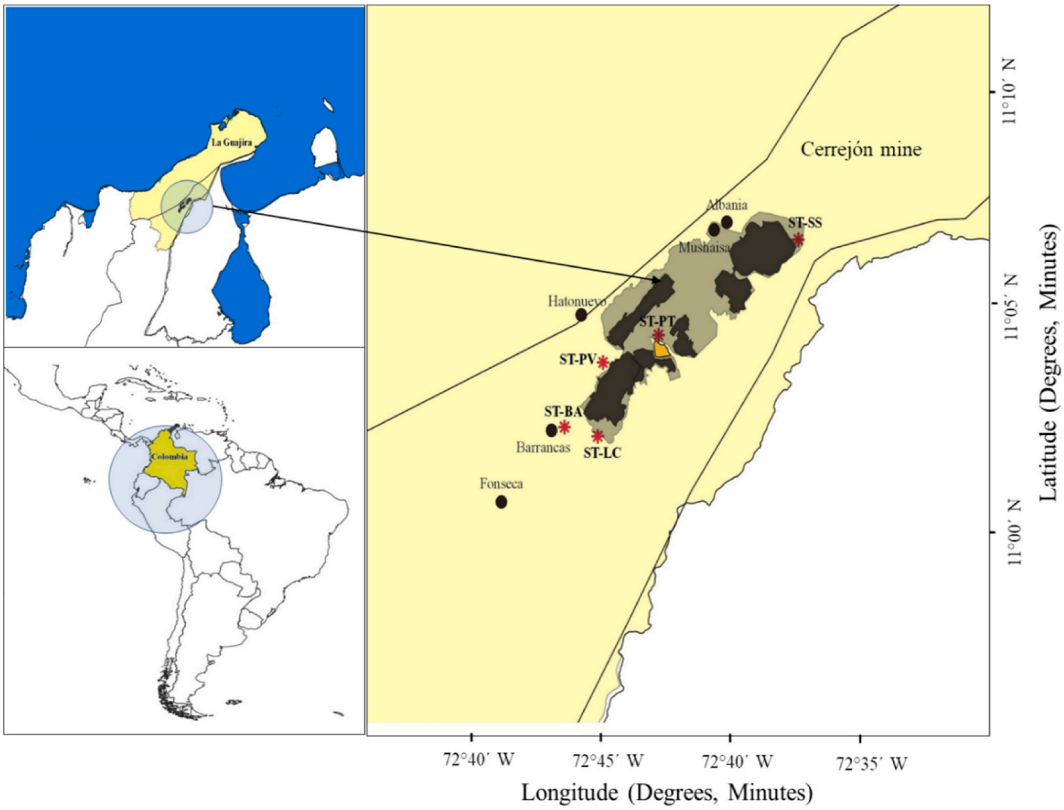

Fig. 1. The geographical location of the Cerrejón coal mine and PM_{10} monitoring stations (Sol y Sombra (ST-SS), Patilla (ST-PT), Provincial (ST-PV), Barrancas (ST-BA), and Las Casitas (ST-LC) stations.

sources. The chemical compounds in PM mass derived from secondary sources include secondary inorganic aerosols. The predominant components of PM_{10} and $PM_{2.5}$ are sulfate (SO_4^{2-}), ammonium (NH_4^+), and nitrate (NO_3^-) ions [25]. Water-soluble ions are the main components of atmospheric aerosols, accounting for more than 10% of PM_{10} mass [26,27]. In cities near coal mines, water-soluble ions are the major PM components. Studies have recorded considerable water-soluble ion concentrations (30%) in PM mass [28,29]. Water-soluble ions, especially sulfate, have a significant impact on air quality and climate in various contexts. The role of aerosols in the atmosphere to scatter incoming radiation is well known [30,31]. Long life in the atmosphere prolongs their impact. Aerosol emission sources are associated with particulate matter, marine aerosols, biomass burning, urban emissions, and emissions from industrial processes. The optical properties of aerosols have allowed their efficient observation from satellites [32,33].

The use of satellite information platform has been very useful in producing daily forecasts of pollutants and aerosols across the globe. The Copernicus Atmosphere Monitoring Service (CAMS) (http://atmosphere.copernicus.eu) provides daily forecasts of aerosol concentrations [34]. This information helps assess the impact of aerosols on air quality [35,36]. Studies have also evaluated surface data measured with satellite data for water-soluble ions, especially sulfate and nitrate. The results showed 26.88% uncertainty for sulfate and 25.55% uncertainty for nitrate at a resolution of $0.1^\circ \times 0.1^\circ$ [37].

CAMS service applies principles and laws of physics and atmospheric chemistry to estimate the concentrations of all species during the study period. The results are validated with the emission estimates or surface observations as a boundary condition. The resolution

Table 1
Location and elevation of the Cerrejón Air Quality Network and meteorological instruments used in this research (Fig. 1). (ST-BA: Barrancas; ST-LC: Las Casitas; ST-PT: Patilla; ST-PV: Provincial; ST-SS: Sol y Sombra).

ID	Stations	Latitude (°)	Longitude (°)	Elevation (m)	Variables
ST-SS	Sol y Sombra	11°8′37.88″ N	72°30′36.64″ W	117	PM_{10}
ST-PT	Patilla	11°30′00″ N	72°40′15.60″ W	115	PM_{10}
ST-PV	Provincial	11°1′23.12″ N	72°44′5.99″ W	156	PM_{10}, T, P, ws, and wd
ST-BA	Barrancas	10°57′34.38″ N	72°46′45.52″ W	150	PM_{10}, T, P, ws, and wd
ST-LC	Las Casitas	10°57′1.69″ N	72°44′28.23″ W	162	PM_{10}, T, P, ws, and wd

of approximately 40 km (approximately 0.35°) [38,39]. In the study, only air quality stations located outside the 40 km range are selected. The model returns an analysis of concentrations every 6 h. The daily average sulfate was determined to be consistent with the corresponding time period for which surface concentrations were measured.

Colombia ranks fifth among coal exporters globally. In 2018, Colombian coal production reached 84.3 Mt. Approximately 90% of the country's coal production is concentrated in the north. In the department of La Guajira, the study area, coal production reached 30.7 Mt in 2018. Mining operations have a positive economic impact in the region but may also be the cause of adverse environmental effects.

In this study, a six-month monitoring program was developed at six stations located in the Cerrejón open-pit coal mine, in the department of La Guajira in northern Colombia, to measure the concentrations of ions dissolved in PM_{10} and to investigate the temporal variations and possible sources of these species. The results of this study may provide useful information to establish control strategies for preventing aerosol contamination in sites near open-pit mines.

2. Materials and methods

2.1. Study area

This study was conducted in the area of affected by the Cerrejón mine (11° 5′ N, 72° 40′ W; Fig. 1). Cerrejón is an open-pit coal mine located in the peninsula of La Guajira in northeastern Colombia, very close to the border with Venezuela. It spans the municipalities of Albania, Hatonuevo, and Barrancas and is 150 km from the Caribbean coast, 100 km from Riohacha, the capital of La Guajira, and 400 km from the industrial city of Barranquilla. The Cerrejón mine is located 85–192 m above sea level and has an intervention area of ~142 km^2. According to projections by the National Administrative Department of Statistics [40], the total population of the department of La Guajira was approximately 1,067,063 inhabitants in 2019. There are 80,312 people living in the area of influence of the coal mine (34% of the population is indigenous). About 70% of this population is located less than 10 km from the extraction site [41].

The terrain is characterized as an alluvial plain located in the Rancheria River basin, between the mountainous ranges of the Serranía de Perijá to the east and the Sierra Nevada de Santa Marta to the west. The coal deposits are located in an area of approximately 80,000 ha. At Cerrejón, coal is extracted from a maximum depth of 200 m below the ground surface. In 2016, the total coal production reached 31.6 Mt, with total exports surpassing 32.4 Mt [42]. Expansion plans to increase the production of the mine to 42 Mt were approved in 2017. The mining operations are performed in the following 6 areas, from north to south: Patilla pit (PATp), 100 pit (100p), Comunero pit (COMp), Oreganal pit (OREp), Tabaco pit (TABp), and La Puente pit (LPUp) (Fig. 1). The climate is strongly affected by the proximity to the mountainous ranges of Serranía de Perijá and Sierra Nevada de Santa Marta. Temperatures range from 13 to 37 °C, averaging 29 °C annually. Wind speeds range from 2.53 to 6.04 m/s, averaging 3.11 m/s annually and predominantly from the NE [43]. The study area experiences dry and rainy seasons based on precipitation presence or absence. There are two rainy seasons, one between April and May (with 1000–1300 mm precipitation) and the other between September and December (precipitation higher than 1100 mm). Conversely, the dry seasons span from January to February (precipitation lower than 450 mm) and from June to August (450–500 mm precipitation).

2.2. Sampling sites

The meteorological variables (temperature (T), relative humidity (RH), precipitation (P), and wind speed (ws) and direction (wd)) and ambient PM_{10} concentrations used in the analysis were assessed at stations of the Cerrejón Air Quality Network (https://www.cerrejon.com/en/sustainability/environment/air). The selected stations are located in the North (Sol y Sombra (ST-SS) station), Central (Patilla (ST-PT) and Provincial (ST-PV) stations), South (Barrancas (ST-BA), and Las Casitas (ST-LC) stations) Zones. Table 1 presents the sampling stations, their geographical location, and the variables measured in this study. ST-SS and ST-BA were the reference stations upwind and downwind of the mining operations (based on prevailing winds). The ST-PT, ST-PV, and ST-LC stations are located in the heart of industrial activities. Additionally, ST-PV and ST-LC are affected by other activities performed by the inhabitants in areas adjacent to these stations. Meteorological data were recorded in only three of the five stations, namely, the Provincial (ST-PV), Barrancas (ST-BA), and Las Casitas (ST-LC) stations. In summary, these five stations cover the entire study area and encompass the main mining activities, as well as other activities in adjacent areas that may interact with and be affected by PM emissions.

Table 2
Statistical summary of meteorological variables (temperature, relative humidity, rainfall and wind speed) measured at selected sites of Cerrejón mine (sites ST-PV, ST-BA, ST- LC).

ID-Station	Temperature (°C)				Relative humidity (%)			
	Mean	SD	Min	Max	Mean	SD	Min	Max
ST-SS	28.22	2.80	12.80	34.80				
ST-PT	29.82	2.01	13.25	36.82				
ST-PV	29.23	1.83	12.80	34.80	59.15	10.23	18.00	96.33
ST-BA	28.89	1.72	25.13	33.17	64.75	10.68	38.66	92.18
ST-LC	29.69	1.97	13.25	36.82	64.01	10.80	18.00	96.20
ID-Station	Rainfall (mm)				ws (m/s)			
	Mean	SD	Min	Max	Mean	SD	Min	Max
ST-SS	1.60	7.64	4.56	119.20	2.66	0.95	0.30	5.39
ST-PT	1.50	6.66	1.23	76.60	2.54	0.96	0.18	6.04
ST-PV	1.84	7.61	1.10	76.60	2.89	1.11	0.00	5.71
ST-BA	1.93	7.73	3.45	110.30	2.83	1.02	0.00	5.24
ST-LC	1.85	7.56	2.67	107.20	3.06	1.11	0.00	5.71

2.3. $p.m._{10}$ concentrations

PM_{10} samples were collected from June to December 2015 using TE-6070 high-volume (Hi-Vol) PM_{10} air samplers purchased from Tisch Environmental (Cleves, OH, USA), equipped with 2 μm Whatman® quartz air sampling filters (8 × 10 in) purchased from Sigma-Aldrich. "The hi-vol PM10 sampler was operated for 24 h with a volumetric flow rate between 1.1 and 1.7 m3/min (36–40 ft3/min)." Daily samples were collected every three days, totaling 210 $p.m._{10}$ samples, distributed as follows: 50 at ST-SS, 49 at ST-PT, 27 at ST-PV, 51 at ST-BA, and 33 at ST-LC. All samples were processed and analyzed using gravimetric techniques, following the reference methods of the Code of Federal Regulations (Appendix J to Part 50 for PM_{10}) [44,45]. Each filter was weighed on an Ohaus EX125D analytical balance (Parsippany, NJ, USA), accurate to 0.01 mg, before and after storing at 30 ± 10% RH and 20 ± 2 °C for 24 h to calculate the difference in weight between the clean and exposed filters. The results were used to determine the concentrations. The QA/QC procedures have been used in all monitoring stations.".

2.4. Ion analysis

The concentrations of four anions (Cl^-, NO_3^-, PO_4^{3-}, and SO_4^{2-}) and five cations (Na^+, NH_4^+, K^+, Mg^{2+}, and Ca^{2+}) were determined for 210 quartz filter samples. The filters were placed in a muffle furnace for 16 h at 550 °C. To extract water-soluble ions, a disk 47 mm in diameter was punched out of each of the 8" × 10″ quartz air sampling filters. These disks were immersed in 30 ml of ultrapure water and 100 μl of pure ethanol. A Dionex DX-500 Ion Chromatography System (Dionex Corporation, Sunnyvale, CA, USA) was used to determine the concentrations of cations and anions in the quartz air sampling filters. The cations were analyzed by gradient separation on an Ionpac CS12A column using 22 mM H_2SO_4 as the eluent. This procedure is described in Research Triangle Institute: 'Standard Operating Procedure for $PM_{2.5}$ Cation Analysis [46]. Similarly, anions were separated on an Ionpac AS4A-SC column using 2.7 mM Na_2CO_3/0.3 mM $NaHCO_3$ as the eluent. This procedure is described in the Research Triangle Institute Standard Operating Procedure for $PM_{2.5}$ Anion Analysis [47]. The resulting ionic mass values were scaled based on the ratio between the perforated and total filter areas.

2.5. Sulfate AOD (550 nm)

In this study, the sulfate concentration in PM_{10} correlated with the sulfate aerosol optical depth at 550 nm (suaod550) in the study area. suaod550 data were downloaded from the Atmosphere Data Store of the Copernicus Atmosphere Monitoring Service (CAMS), ECMWF. Programmatic access to the data was provided by the Climate Data Store Application Program Interface (CAMS global atmospheric composition forecasts). CAMS forecast data have a resolution of approximately 40 km (approximately 0.35°). The horizontal resolution of the satellite data covered three stations (grid size of about 40 km). Were considered for the study, the stations impacted by regional sources (ST-SS) and extractive operations (ST-BA). suaod550 data were initially interpolated to the coordinates of the ST-SS, and ST-BA stations (North, and South Zones of the mine). These data were downloaded every 3 h from 00:00 UTC to 21:00 UTC. At each station, 24 h averages were calculated, coinciding with the sampling times of the surface data.

2.6. Data analysis

Data analysis was performed with Microsoft® Excel® 2019 MSO (Microsoft Corporation, Santa Rosa, CA). The correlation between of the ions in PM_{10} was retrieved using Pearson's coefficients. The R packages (r-studio) (OpenAir air quality tool) were used for computing the Polar plot of concentrations of the main ions [48]. The Python 3.10.9 (Packaged by Anaconda, Inc.) (https://docs.anaconda.com/free/navigator/) was used to analyze the sulfate aerosol optical depth at 550 nm (suaod550) in the study area.

Table 3
Mean PM_{10} concentrations, standard deviation (SD), maxima and minima, and confidence interval at each station (the matrix of all data).

Station	N	Mean (μg/m^3)	SD (μg/m^3)	Maximum (μg/m^3)	Minimum (μg/m^3)	$CI_{95\%}$
ST-SS	50	20.48	9.16	38.37	5.55	2.58
ST-PT	49	40.89	13.63	95.31	14.40	3.76
ST-PV	27	31.48	13.54	74.29	15.83	5.08
ST-BA	51	41.98	17.53	89.06	12.15	5.10
ST-LC	33	53.20	19.88	95.03	15.26	6.75
All	210	36.93	18.41	95.03	5.55	2.52

Table 4
Concentrations of water-soluble inorganic ions in PM_{10} at sampling stations.

Station		Na^+	Ions	(μg/m^3)	($N = 210$)	Ca^{2+}	Cl^-	NO_3^-	PO_4^{3-}	SO_4^{2-}
			NH_4^+	K^+	Mg^{2+}					
	Mean	0.54	0.41	0.06	0.06	0.16	0.14	0.22	0.12	2.16
	SD	0.18	0.36	0.03	0.02	0.05	0.17	0.12	0.02	1.02
ST-SS	Max	0.95	1.89	0.18	0.11	0.31	0.65	0.47	0.19	5.91
($n = 50$)	Min	0.12	0.00	0.01	0.03	0.05	0.00	0.02	0.09	0.03
	$CI_{95\%}$	0.05	0.10	0.01	0.01	0.01	0.05	0.03	0.01	0.28
	Mean	1.27	0.37	0.09	0.17	0.37	0.94	0.63	0.14	2.65
	SD	1.14	0.43	0.09	0.15	0.35	1.17	0.60	0.08	2.44
ST-PT	Max	5.13	2.27	0.39	0.72	1.98	5.00	2.62	0.52	9.83
($n = 49$)	Min	0.07	0.01	0.01	0.01	0.01	0.01	0.02	0.06	0.01
	$CI_{95\%}$	0.32	0.12	0.02	0.04	0.10	0.33	0.17	0.02	0.68
	Mean	0.80	0.47	0.06	0.09	0.23	0.44	0.37	0.13	2.73
	SD	0.45	0.36	0.04	0.06	0.15	0.45	0.18	0.05	1.50
ST-PV	Max	1.84	1.32	0.16	0.23	0.76	1.78	0.81	0.33	6.29
($n = 27$)	Min	0.10	0.00	0.00	0.00	0.04	0.02	0.04	0.09	0.00
	$CI_{95\%}$	0.17	0.13	0.01	0.02	0.06	0.17	0.07	0.02	0.56
	Mean	1.20	0.67	0.11	0.16	0.40	0.74	0.64	0.13	3.94
	SD	0.62	0.48	0.05	0.08	0.22	0.67	0.27	0.03	1.85
ST-BA	Max	2.39	2.24	0.24	0.34	1.01	2.40	1.07	0.18	9.02
($n = 51$)	Min	0.09	0.00	0.01	0.01	0.04	0.01	0.02	0.08	0.00
	$CI_{95\%}$	0.17	0.13	0.01	0.02	0.06	0.18	0.07	0.01	0.51
	Mean	2.06	1.37	0.20	0.28	0.62	0.91	0.88	0.79	7.04
	SD	3.58	1.47	0.33	0.51	1.22	1.20	0.91	3.52	5.65
ST-LC	Max	21.00	7.43	1.80	3.00	7.20	5.40	4.80	20.40	32.40
($n = 33$)	Min	0.09	0.00	0.01	0.02	0.03	0.01	0.03	0.09	0.00
	$CI_{95\%}$	1.22	0.50	0.11	0.17	0.41	0.41	0.31	1.20	1.92

3. Results and discussion

3.1. Meteorology and PM_{10} concentrations

Meteorological variables were measured at three selected locations (ST-PV, ST-BA, ST-LC) (Table 2). The average temperature was 29.49 °C, with an average annual RH of 65%. Wind speed recorded values between 2 and 5 m/s, with predominant winds from the NNE, NEE, and NE. The rainy season occurs twice a year, from April to May (the first rainy season) and from October to December (the second rainy season). The remaining months of the year are considered the dry period. The average annual rainfall was recorded as 400 mm during the study period. The existence of uniform meteorological characteristics was estimated in the same area. Table 3 outlines the mean concentrations, number of samples, standard deviation (SD), maxima and minima, and confidence interval at each station, i.e., the matrix of all the data. All the devices were operated under the same characteristics, according to the manufacturer's instructions. The overall mean of all stations was 36.93 μg/m^3 ($CI_{95\%}$, 34.41–39.45), with an SD of 18.41 μg/m^3. ST-LC had the highest mean PM_{10} concentration, at 53.20 μg/m^3 ($CI_{95\%}$, 46.46–59.95), with an SD of 19.88 μg/m^3, followed by ST-BA, with a mean of 41.98 μg/m^3 ($CI_{95\%}$, 36.89–47.08) and an SD of 17.53 μg/m^3. ST-PT had a mean of 40.89 μg/m^3 ($CI_{95\%}$, 37.14–44.65) and an SD of 13.63 μg/m^3. ST-PV had a mean of 31.48 μg/m^3 ($CI_{95\%}$, 26.40–36.56) and an SD of 13.54 μg/m^3. Lastly, ST-SS had the lowest mean, at 20.48 μg/m^3 ($CI_{95\%}$, 17.90–23.06), and an SD of 9.16 μg/m^3.

These results are in line with the findings of other studies in the same area [49,50]. The mean PM_{10} concentrations did not exceed the daily (100 μg/m^3) and annual (50 μg/m^3) average maximum permissible levels of PM_{10} established in the Colombian standard, in any station [51]. However, all mean PM_{10} concentrations at ST-BA, ST-LC, ST-PT, and ST-PV exceeded the annual permissible limit (15 μg/m^3) of the 2021 WHO air quality guidelines (AQGs) during the study period [1]. An analysis of the results also showed that 4%, 11%, 20%, 13%, and 25% of the PM_{10} concentrations assessed at the ST-SS, ST-PT, ST-PV, ST-BA, and ST-LC stations, respectively,

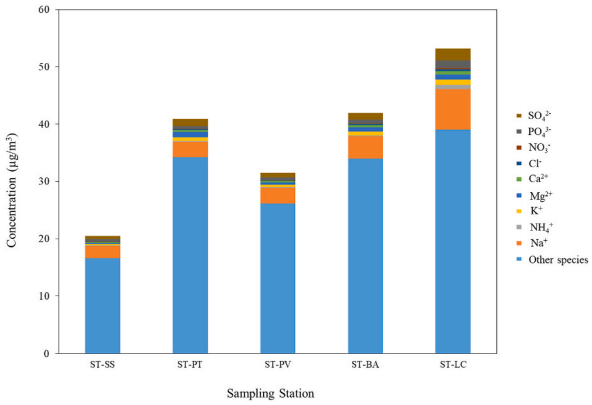

Fig. 2. Concentration of water-soluble ions in PM_{10} (μg/m^3) in open-pit coal mines from June to December 2017. Sol y Sombra (ST-SS), Patilla (ST-PT), Provincial (ST-PV), Barrancas (ST-BA), and Las Casitas (ST-LC) stations.

exceeded the 24 h average PM_{10} threshold of the 2021 WHO AQGs (45 μg/m^3). PM_{10} concentrations at station ST-SS, located upwind of the mining activities, indicated significant contribution from regional sources. Stations ST-PT, ST-PV, ST-BA, and ST-LC indicated direct contribution from open-pit mining activities. Section 3.2 details the possible sources of PM_{10} in the study area.

3.2. Concentration of anions and cations in receptors

In the present study, 210 PM_{10} samples were analyzed to determine the mass of anions and cations. SO_4^{2-}, Na^+, and NH_4^+ were the ions with the highest concentrations. Combined, these three ions accounted for 75% of the total PM_{10} mass of the 210 samples. The remaining 25% of PM_{10} mass comprising K^+, Mg^{2+}, Ca^{2+}, Cl^-, NO_3^-, and PO_4^{3-}. Table 4 outlines the mean concentrations of water-soluble inorganic ions in PM_{10} at the ST-SS, ST-PT, ST-PV, ST-BA, and ST-LC stations. The mean concentration of SO_4^{2-} was 3.55 μg/m^3 ($CI_{95\%}$, 3.12–4.00), with an SD of 3.21 μg/m^3. The maximum 24 h concentration (32.40 μg/m^3) was recorded on December 9 and the lowest value (0.01 μg/m^3) was recorded on December 25. Na^+ concentrations ranged from 0.09 to 21.00 μg/m^3, and the overall mean was 1.14 μg/m^3 ($CI_{95\%}$, 0.92–1.36). NH_4^+ concentrations ranged from 0.01 to 7.43 μg/m^3, averaging 0.62 μg/m^3 ($CI_{95\%}$, 1.09–1.42). The mean concentrations of K^+, Mg^{2+}, Ca^{2+}, Cl^-, NO_3^-, and PO_4^{3-} were 0.10 ($CI_{95\%}$, 0.08–0.12), 0.15 ($CI_{95\%}$, 0.12–0.18), 0.35 ($CI_{95\%}$, 0.27–0.42), 0.63 ($CI_{95\%}$, 0.52–0.75), 0.54 ($CI_{95\%}$, 0.47–0.61), and 0.24 ($CI_{95\%}$, 0.05–0.42) μg/m^3, respectively. The ranges of these data are similar to those reported for mining areas of the department of Cesar, located farther south of Cerrejón [52]. However, they significantly differed from the results of measurements performed in the same study area in another study [28].

The highest means and maximum values of the concentrations of the nine ions under study were recorded at ST-LC. The lowest mean concentrations of SO_4^{2-}, Na^+, K^+, Mg^{2+}, Ca^{2+}, Cl^-, NO_3^-, and NH_4^+ and PO_4^{3-} were recorded at ST-SS and ST-PT, respectively. The lowest values of all ion concentrations were recorded at ST-SS. These results clearly show a greater input of inorganic ions at ST-LC, which also had the highest PM_{10} values. On average, these nine ions accounted for 19.65% ($CI_{95\%}$, 18.29–20.91) of the PM_{10} mass during the study period. On two days, the mass of ions accounted for more than 50% of the PM_{10} mass. The daily mean concentrations of ions were somewhat similar to the PM_{10} concentrations, although with some differences in various ions and stations. Based on the means, the three main water-soluble inorganic species (SO_4^{2-}, Na^+, and NH_4^+) accounted for 20.45% of the PM_{10} mass. Combined, these three elements accounted for 75% of the total concentrations of ions in this study (Fig. 2).

Fig. 3 shows the temporal variation in the concentrations of the main ions, namely, SO_4^{2-}, Na^+, and NH_4^+, in PM_{10}, at the ST-SS, ST-PT, ST-PV, ST-BA, and ST-LC monitoring stations. Except for Cl^-, all other ions had higher means in the dry seasons than in the rainy seasons. However, no significant difference ($p > 0.05$) was found between the means of all stations in the dry and rainy seasons by analysis of variance. These nonsignificant differences may be normal because precipitation can remove aerosols from the atmosphere; however, aerosols can be quickly recharged after rainfall events [53].

The relationships between the anions and cations are graphically represented in Fig. 4, which shows a high correlation coefficient between anion and cation concentrations ($r = 0.95$). These results confirm that the ions were derived from a common source. Overall, the mean concentration of anions (4.96 μg/m^3, $CI_{95\%}$: 2.56–3.74) was higher than the mean concentration of cations (2.36 μg/m^3, $CI_{95\%}$: 1.98–2.74). The mean concentrations of the ions decreased in the following order: $SO_4^{2-} > Na^+ > NH_4^+ > Cl^- > NO_3^- > PO_4^{3-} > Ca^{2+} > K^+ > Mg^{2+}$. These results suggest that the main source of the three main ions may be coal combustion. The high correlation suggests that the precursors of these species were released from similar emission sources, such as coal burning, vehicle exhausts, the industrial sector, and natural and anthropogenic mineral dust [54,55].

Table 5 outlines the Pearson product-moment correlation coefficients of the total concentrations of ions in PM_{10} at all stations. ST-LC had the highest correlation values (0.32–0.99), followed by ST-PT. ST-SS had the highest number of negative Pearson product-moment correlation coefficients. By ion species, PO_4^{3-} had only negative coefficients of correlation with other ions. SO_4^{2-} had positive and significant coefficients of correlation with NH_4^+ and NO_3^- ($r = 0.76$ and 0.57), indicating that a fraction of these ions may have derived from a similar source. Ca^{2+} and Mg^{2+} are major soil components. These ions showed a good coefficient of correlation with each

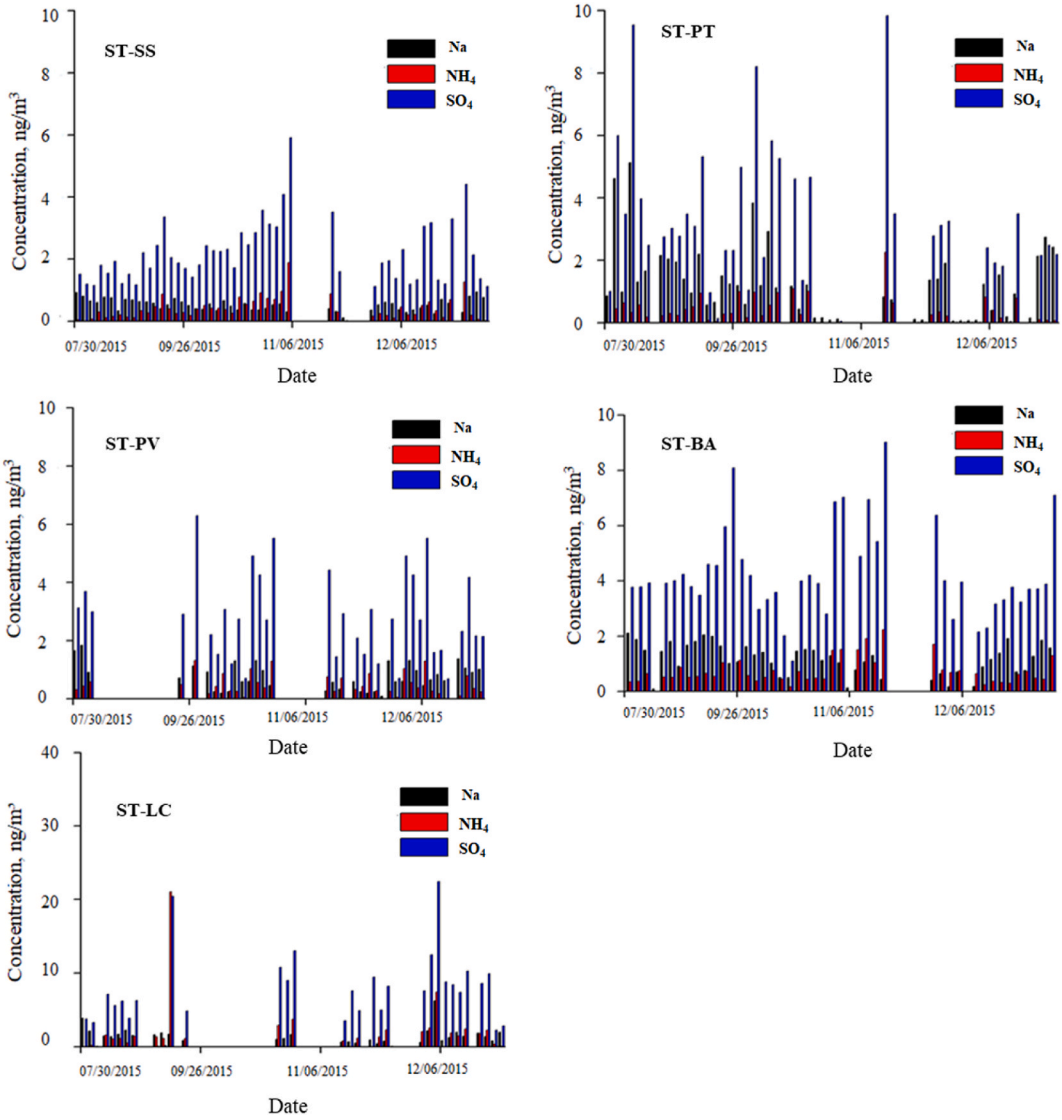

Fig. 3. Temporal variation in the concentrations of the main ions: SO_4^{2-}, Na^+, and $NH4^+$ in PM_{10} at the monitoring stations. Sol y Sombra (ST-SS), Patilla (ST-PT), Provincial (ST-PV), Barrancas (ST-BA), and Las Casitas (ST-LC) stations.

other ($r = 0.89$), suggesting that they also have a common source.

The relationships between NH_4^+, Mg^{2+}, Ca^{2+}, Cl^-, Na^+, and K^+ may also indicate a similar source. The relationship between Na^+ and Cl^- ($r = 0.89$) is indicative of salt from marine aerosols [27,56]. These ions have a high correlation coefficient ($r = 0.89$), which indicates the contribution of the Caribbean coast to PM_{10} in the Cerrejón mine. The correlation between Na^+ and K^+ ($r = 0.60$) reflects the influence of agricultural activities [26]. The correlation coefficient was high for all samples; however, their correlation analysis by the station showed that ST-LC had the highest coefficient ($r = 0.85$), suggesting that sources of emissions from agricultural activities influenced the results assessed at this station. The levels of potassium ions (K^+) were higher at ST-LC than at other stations. In PM_{10}, this ion species is a marker of biomass burning emissions, and its levels at this station could be related to emissions from artisan stoves used by the inhabitants of this community for their domestic activities. Broadly speaking, the relationships between ion concentrations in the mining area showed a positive and significant correlation for most paired ions, with 60% of paired samples showing a Pearson product-moment correlation coefficient ranging from 0.48 to 0.98. A simple explanation for these relationships is the common origin of the ions. Their emissions must derive from similar and local sources, more specifically, coal mining activity [53,57].

3.3. Marine contribution to aerosol composition

The open-pit coal mining area in northern Colombia is close to the Caribbean Sea. This zone can be influenced by marine aerosols [58,59]. Considering this sea-mine proximity, the contribution of sea salt to soluble ions in PM_{10} was assessed in the mining area. The

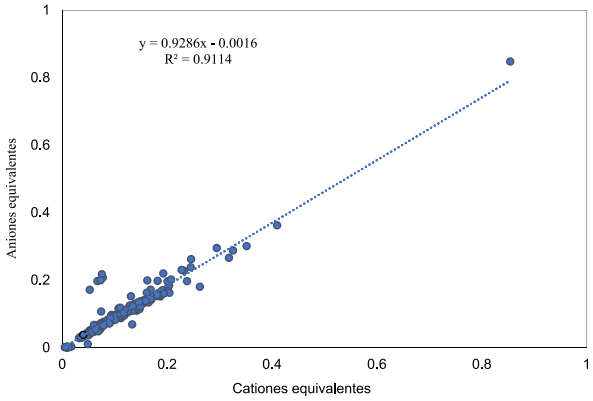

Fig. 4. Linear regression between anions and cations presents in PM_{10} at all stations of the study area. Sol y Sombra (ST-SS), Patilla (ST-PT), Provincial (ST-PV), Barrancas (ST-BA), and Las Casitas (ST-LC) stations.

Table 5
Pearson Correlation Coefficient (R) of the concentrations of the ions in PM_{10} assessed at five monitoring stations of the Cerrejón coal mine.

	Na^+	NH_4^+	K^+	Mg^{2+}	Ca^{2+}	Cl^-	NO_3^-	PO_4^{3-}	SO_4^{2-}
Na^+	1	0.10	0.60	0.99	0.86	0.89	0.88	−0.15	0.44
NH_4^+		1	0.23	0.15	0.18	−0.12	0.25	0.25	0.76
K^+			1	0.62	0.59	0.47	0.62	−0.05	0.44
Mg^{2+}				1	0.89	0.88	0.90	−0.17	0.48
Ca^{2+}					1	0.77	0.85	−0.11	0.47
Cl^-						1	0.71	−0.24	0.16
NO_3^-							1	−0.06	0.57
PO_4^{3-}								1	0.20
SO_4^{2-}									1

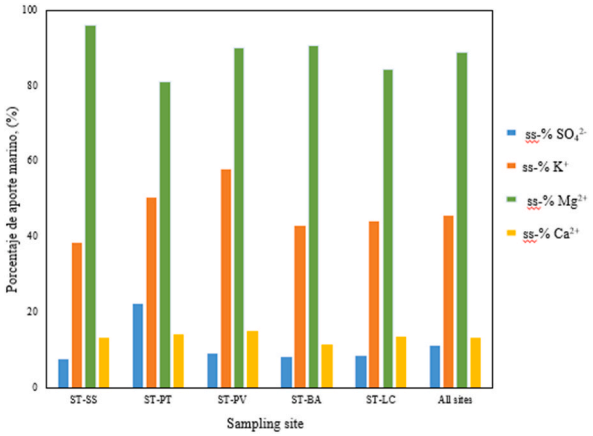

Fig. 5. Proportions of sea-salt (ss)-derived water-soluble ions in PM_{10} by sampling site, namely, ss-SO_4^{2-}, ss-K^+, ss-Mg^{2+}, and ss-Ca^{2+}. Sol y Sombra (ST-SS), Patilla (ST-PT), Provincial (ST-PV), Barrancas (ST-BA), and Las Casitas (ST-LC) stations.

contribution of marine aerosols was estimated assuming that Na^+ is derived from the sea. Under this assumption, the non-sea salt (nss) value of any ion was calculated using the equation established by Cheng et al. [57], with proven results reported by Xu et al. [60], and Zhang et al., [61].

$$nss - x = x_i - Na_i^+ \times \left(x/_{Na^+}\right)_{sea} \quad (1)$$

where x_i and Na_i^+ represent the concentrations of an ion and Na_i^+ in ambient air samples of PM_{10}, respectively. $\left(x/_{Na^+}\right)_{sea}$ is the ratio between the concentration of the ion and the concentration of Na^+ in seawater. According to the seawater composition, $\left(x/_{Na^+}\right)_{sea}$ is 1.81 for X = Cl^-, 0.04 for X = Ca^{2+}, 0.13 for X = Mg^{2+}, 0.04 for X = K^+, and 0.25 for X = SO_4^{2-} [62]. Fig. 5 shows the proportions of

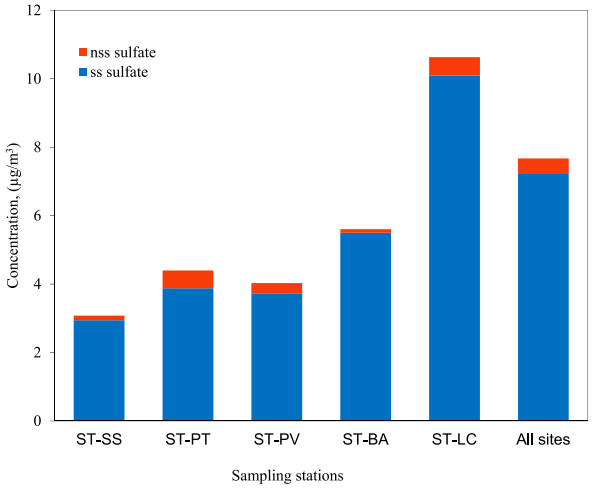

Fig. 6. Concentration of nss sulfate (SO_4^{2-}) in PM_{10} by monitoring station. Sol y Sombra (ST-SS), Patilla (ST-PT), Provincial (ST-PV), Barrancas (ST-BA), and Las Casitas (ST-LC) stations.

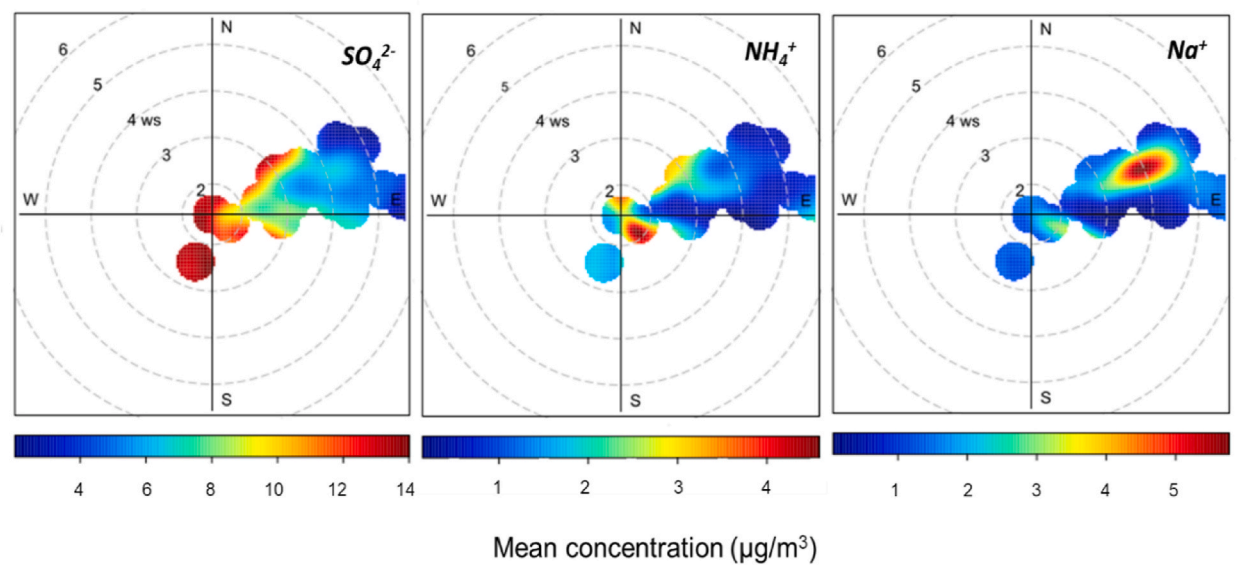

Fig. 7. Polar plot of concentrations of the main ions –SO_4^{2-}, NH_4^+, and Na^+— in PM_{10} at the Las Casitas (ST-LC) monitoring station.

sea-salt (ss)-derived water-soluble ions, namely, ss-SO_4^{2-}, ss-K^+, ss-Mg^+, and ss-Ca^{2+}, at each sampling station. K^+ and Mg^+ showed the highest percentages of marine contribution (88.90% and 45.54%). Conversely, SO_4^{2-} and Ca^{2+} showed the lowest percentages of marine contribution (13.43% and 11.19%).

The ST-LC monitoring station had the highest mean concentration of ions, at 6.52 µg/m^3 (92%), followed by ST-BA at 3.64 µg/m^3 (90%), ST-PT at 2.34 µg/m^3 (78%), ST-PV at 2.28 µg/m^3 (91%), and ST-SS at 2.03 µg/m^3 (68%). These results show that the ST-SS station, located upwind of the mining operations, has the lowest contribution of nss sulfate. Among the ions, sulfate stands out as the component with the highest mass in PM_{10}. The nss sulfate can be estimated using Equation (1) by replacing the value of X in $\left(x/_{Na^+}\right)_{sea}$ with the value of SO_4^{2-}. This sulfate can be generated by spontaneous coal combustion, which commonly occurs in this mine during the rainy season. Some fractions of SO_2 emitted from heterogeneous or homogeneous reactions are oxidized to sulfate aerosols before dry or wet deposition. Based on the application of this equation, the mean concentration of nss-SO_4^{2-} was 3.26 µg/m^3 ($CI_{95\%}$, 2.84–3.68), with an SD of 3.13 µg/m^3. Approximately 71.95% ($CI_{95\%}$, 55.03–80.88) of the SO_4^{2-} mass may have been emitted from tillage and spontaneous combustion of coal seams (Fig. 6).

Fig. 7 shows the polar plot of the concentrations of the main ions, namely, SO_4^{2-}, NH_4^+, and Na^+, in PM_{10} at the SS-LC monitoring station (the station with the highest concentrations). This figure shows high values of SO_4^{2-} and NH_4^+ from the NE wind direction and with speeds lower than 3 m/s, suggesting ion contributions from local sources, possibly from mining activity. The Na^+ concentrations

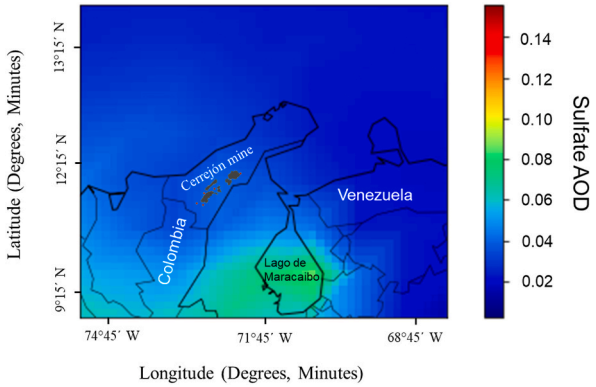

Fig. 8. Daily means of sulfate aerosol optical depth at 550 nm (suaod550) in the Cerrejón coal mine.

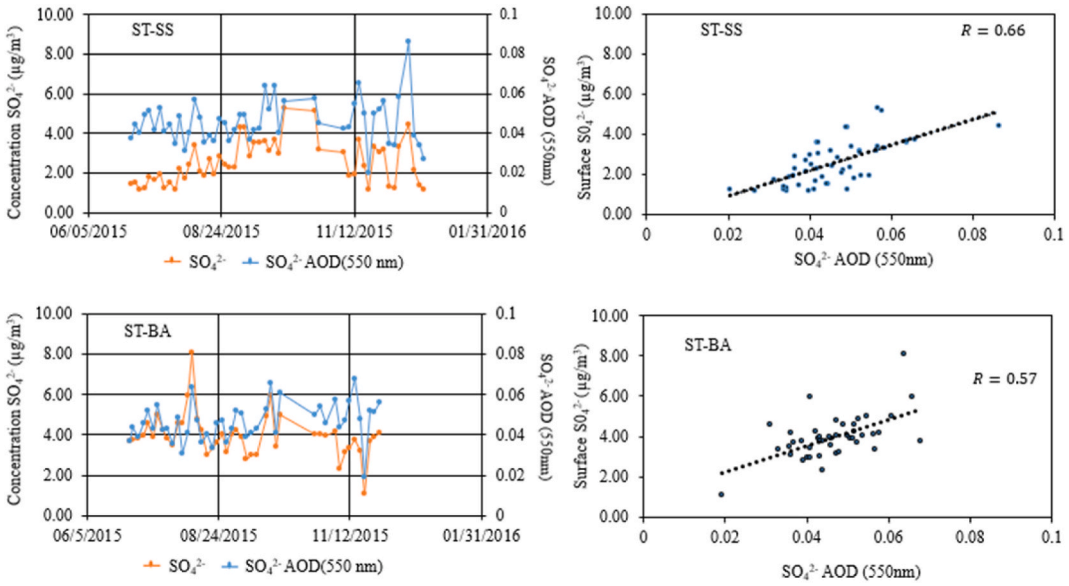

Fig. 9. Temporal variation and correlation between the concentration of sulfate ions (SO_4^{2-} in PM_{10} and sulfate aerosol optical depth at 550 nm (suaod550). Sol y Sombra (ST-SS), Barrancas (ST-BA).

show a wind speed range greater than 4 m/s, suggesting a contribution from regional sources, in addition to local sources, possibly due to the contribution of marine aerosols, given the proximity of the mine to the coast.

3.4. Surface sulfate vs suaod550

Fig. 8 shows the daily means of suaod550, highlighting the strong influence of suaod550 from Venezuela (Lake Maracaibo) on central and northern Colombia. This region is important due to the presence of the oil and petrochemical industry and has high levels of sulfate and chloride [63]. In recent research, Rojano et al. [64], showed that wind trajectories from northwestern Venezuela impact northern and central Colombia. Fig. 9 shows the temporal variation and correlation analysis of the sulfate ion (SO_4^{2-}) in PM_{10} and suaod550 (SO_4^{2-} AOD(550 nm)) based on CAMS data. The ST-SS (located to the north of the study area) and ST-BA stations (located to the south of the study area) showed a consistent pattern in the variability of satellite (suaod550) and surface data of the sulfate ion (SO_4^{2-}) concentration in PM_{10}.

These results show a strong, positive, and linear correlation between the sulfate ions (SO_4^{2-}) in PM_{10} and suaod550 at the monitoring stations. The increase in suaod550 is in line with the increase in sulfate ion (SO_4^{2-}) concentrations in PM_{10}. The correlation between sulfate ions (SO_4^{2-}) and suaod550 (Fig. 9) is considered acceptable at both stations, with $R = 0.66$ at ST-SS and $R = 0.57$ at ST-BA. These results suggest that suaod550 may be used to estimate PM_{10} concentrations in northern Colombia with acceptable accuracy. Previous studies showed a positive and good linear correlation between the concentrations of PM_{10} and satellite values of PM_{10} (AOD550 nm) [65,66]. Although the results obtained in this study correlate the concentration of sulfate ions (SO_4^{2-}) in PM_{10} and

suaod550, positive linearity was also observed for chemical substances contained in PM_{10}.

4. Conclusion

The PM_{10} concentrations measured did not exceed Colombian national air quality standards but exceeded the WHO international guidelines for daily and annual averages for most sites. SO_4^{2-}, Na^+, and NH_4^+ are the most abundant species, accounting for 75% of the ion masses under study. These species contribute to 22.45% of the PM_{10} mass. The sulfate ion stands out as the main component, with the highest mass in PM_{10}. The results showed that the atmosphere influenced by the extractive activity was dominated by SO_4^{2-}, Na^+, and NH_4^+ contributing an average of 20.45% of the PM_{10} mass. The contribution of marine aerosols to K^+ and Mg^+ concentration was higher, while the contribution of sea salt to SO_4^{2-} and Ca^{2+} concentration was comparatively lower.

The mean concentrations of SO_4^{2-} and NH_4^+ are high, from the NE wind direction and with speeds lower than 3 m/s, suggesting ion inputs from local sources. Approximately 71.95% of the ion mass in PM_{10} is emitted from local sources. The concentration of sulfate ions (SO_4^{2-}) in PM_{10} significantly correlates with Sulfate aerosol optical depth at 550 nm (suaod550), data obtained from CAMS Global atmospheric composition forecast. The results emphasize the dependability of atmosphere composition reanalysis information, establishing it as a valuable supplementary resource to air quality observations at surface level. The slight variation between the two stations may be attributed to the horizontal resolution of the CAMS forecast data, which is approximately 40 km (0.35°). The results emphasize the dependability of atmosphere composition reanalysis information, establishing it as a valuable supplementary resource to air quality observations at surface level.

Data availability statement

The data that support the findings of this study are available upon reasonable request from the corresponding author. If you are interested in the data, please get in touch with Roberto Rojano by e-mail at rrojano@uniguajira.edu.co.

CRediT authorship contribution statement

Roberto Rojano: Writing – review & editing, Writing – original draft, Supervision, Investigation. **Heli A. Arregocés:** Writing – review & editing, Software, Investigation. **Gloria Restrepo:** Writing – original draft, Supervision, Investigation.

Declaration of competing interest

The authors declare that they have no known competing financial interests or personal relationships that could have appeared to influence the work reported in this paper.

Acknowledgements

The authors thank the University of Antioquia (Universidad de Antioquia) and the University of La Guajira (Universidad de la Guajira) for their logistical support. The authors thank the Atmosphere Data Store of the Copernicus Atmosphere Monitoring Service (CAMS) for providing access to satellite data.

References

[1] WHO, WHO global air quality guidelines. Particulate matter (PM2.5 and PM10), ozone, nitrogen dioxide, sulfur dioxide and carbon monoxide, World Heal. Organ. (2021) 1–360.
[2] EPA, Particulate Matter (PM), Pollution, U.S. Environ. Prot. Agency, 2021, 1–2, https://www.epa.gov/pm-pollution. (Accessed 17 May 2022).
[3] R. Hu, G. Liu, H. Zhang, H. Xue, X. Wang, R. Wang, Particle-associated polycyclic aromatic hydrocarbons (PAHs) in the atmosphere of hefei, China: levels, characterizations and health risks, Arch. Environ. Contam. Toxicol. 74 (2018) 442–451, https://doi.org/10.1007/s00244-017-0472-z.
[4] M. Baek, J. Jung, T. Jang, S. Kim, K. Ko, Y. Kim, The effect of PM10 on the symptoms of allergic rhinitis during spring, Otolaryngol. Neck Surg. 149 (2013) P257–P258, https://doi.org/10.1177/0194599813496044a349.
[5] P. Torres, J. Ferreira, A. Monteiro, S. Costa, M.C. Pereira, J. Madureira, A. Mendes, J.P. Teixeira, Air pollution: a public health approach for Portugal, Sci. Total Environ. 643 (2018) 1041–1053, https://doi.org/10.1016/j.scitotenv.2018.06.281.
[6] E.J. Park, C. Yoon, J.S. Han, G.H. Lee, D.W. Kim, E.J. Park, H.J. Lim, M.S. Kang, H.Y. Han, H.J. Seol, K.P. Kim, Effect of PM10 on pulmonary immune response and fetus development, Toxicol. Lett. 339 (2021) 1–11, https://doi.org/10.1016/j.toxlet.2020.11.024.
[7] Z.S. Motesaddi, M. Hadei, S.S. Hashemi, E. Shahhosseini, P.K. Hopke, Z. Namvar, A. Shahsavani, Effects of ambient air pollutants on hospital admissions and deaths for cardiovascular diseases: a time series analysis in Tehran, Environ. Sci. Pollut. Res. 29 (2022) 17997–18009, https://doi.org/10.1007/s11356-021-17051-y.
[8] J. Portugal-Pereira, A. Koberle, A.F.P. Lucena, P.R.R. Rochedo, M. Império, A.M. Carsalade, R. Schaeffer, P. Rafaj, Interactions between global climate change strategies and local air pollution: lessons learnt from the expansion of the power sector in Brazil, Clim. Change 148 (2018) 293–309, https://doi.org/10.1007/s10584-018-2193-3.
[9] I.J. Chaudhary, D. Rathore, Suspended particulate matter deposition and its impact on urban trees, Atmos. Pollut. Res. 9 (2018) 1072–1082, https://doi.org/10.1016/j.apr.2018.04.006.
[10] S. Sun, L. Tian, W. Cao, P.-C. Lai, P.P.Y. Wong, R.S. Lee, T.G. Mason, A. Krämer, C.-M. Wong, Urban climate modified short-term association of air pollution with pneumonia mortality in Hong Kong, Sci. Total Environ. 646 (2019) 618–624, https://doi.org/10.1016/j.scitotenv.2018.07.311.
[11] P.K. Rai, Impacts of particulate matter pollution on plants: implications for environmental biomonitoring, Ecotoxicol. Environ. Saf. 129 (2016) 120–136, https://doi.org/10.1016/j.ecoenv.2016.03.012.

[12] L. Espitia-Pérez, J. da Silva, P. Espitia-Pérez, H. Brango, S. Salcedo-Arteaga, L.S. Hoyos-Giraldo, C.T. de Souza, J.F. Dias, D. Agudelo-Castañeda, A. Valdés Toscano, M. Gómez-Pérez, J.A.P. Henriques, Cytogenetic instability in populations with residential proximity to open-pit coal mine in Northern Colombia in relation to PM10 and PM2.5 levels, Ecotoxicol. Environ. Saf. 148 (2018) 453–466, https://doi.org/10.1016/j.ecoenv.2017.10.044.
[13] S. Gautam, A.K. Patra, S.P. Sahu, M. Hitch, Particulate matter pollution in opencast coal mining areas: a threat to human health and environment, Int. J. Min. Reclamat. Environ. 32 (2018) 75–92, https://doi.org/10.1080/17480930.2016.1218110.
[14] A.K. Patra, S. Gautam, P. Kumar, Emissions and human health impact of particulate matter from surface mining operation-A review, Environ. Technol. Innov. 5 (2016) 233–249, https://doi.org/10.1016/j.eti.2016.04.002.
[15] B.M. Barnes, The Health Impacts of Coalmining Operations and Coal Combustion on Geographically Proximate, 2012.
[16] M.S. Hendryx, M.M. Ahern, T.R. Nurkiewicz, Hospitalization patterns associated with Appalachian coal mining, J. Toxicol. Environ. Health, Part A 70 (2007) 2064–2070, https://doi.org/10.1080/15287390701601236.
[17] M. Hendryx, M.M. Ahern, Mortality in Appalachian coal mining regions: the value of statistical life lost, Publ. Health Rep. 124 (2009) 541–550.
[18] M. Hendryx, M.M. Ahern, Relations between health indicators and residential proximity to coal mining in West Virginia, Am. J. Publ. Health 98 (2008) 669–671, https://doi.org/10.2105/AJPH.2007.113472.
[19] E.S. Bernhardt, B.D. Lutz, R.S. King, J.P. Fay, C.E. Carter, A.M. Helton, D. Campagna, J. Amos, How many mountains can we mine? Assessing the regional degradation of central appalachian rivers by surface coal mining, Environ. Sci. Technol. 46 (2012) 8115–8122, https://doi.org/10.1021/es301144q.
[20] M. Hendryx, K.A. Innes-Wimsatt, Increased risk of depression for people living in coal mining areas of central Appalachia, Ecopsychology 5 (2013) 179–187, https://doi.org/10.1089/eco.2013.0029.
[21] W.D. Jenkins, W.J. Christian, G. Mueller, K.T. Robbins, Population cancer risks associated with coal mining: a systematic review, PLoS One 8 (2013) 1–12, https://doi.org/10.1371/journal.pone.0071312.
[22] M. Hendryx, The public health impacts of surface coal mining, Extr. Ind. Soc. 2 (2015) 820–826, https://doi.org/10.1016/j.exis.2015.08.006.
[23] G.S. Mueller, A.L. Clayton, W.E. Zahnd, K.M. Hollenbeck, M.E. Barrow, W.D. Jenkins, D.R. Ruez, Manuscript title: geospatial analysis of Cancer risk and residential proximity to coal mines in Illinois, Ecotoxicol. Environ. Saf. 120 (2015) 155–162, https://doi.org/10.1016/j.ecoenv.2015.05.037.
[24] S.M. Woolley, A.O. Youk, T.M. Bear, L.C. Balmert, E.O. Talbott, J.M. Buchanich, Impact of coal mining on self-rated health among appalachian residents, J. Environ. Public Health 2015 (2015), https://doi.org/10.1155/2015/501837.
[25] M. Manousakas, E. Diapouli, C. Belis, V. Vasilatou, M. Gini, F. Lucarelli, X. Querol, K. Eleftheriadis, Quantitative assessment of the variability in chemical profiles from source apportionment analysis of PM10 and PM2.5 at different sites within a large metropolitan area, Environ. Res. 192 (2021), https://doi.org/10.1016/j.envres.2020.110257.
[26] E.M. Fujita, Ambient Monitoring and Source Apportionment, 2000, pp. 1–68.
[27] J.G. Watson, J.C. Chow, L.W.A. Chen, G. Engling, X.L. Wang, Source apportionment: principles and methods, in: Issues Environ. Sci. Technol., 2016, pp. 72–125, https://doi.org/10.1039/9781782626589-00072.
[28] C.D. Argumedo, J.F. Castillo, Chemical characterization of particulated atmospheric matter PM10 in Guajira, Colombia, Rev. Colomb. Quím. 45 (2016) 19–29, https://doi.org/10.15446/rev.colomb.quim.v45n2.56991.
[29] A. Hernadez, N. Rojas, Chemical characterization of particulate matter in cesar coal mining region, in: 4TH Colomb. Meet. Int. Conf. AIR Qual, . PUBLIC Heal., 2012, pp. 67–73, https://doi.org/10.1007/BF00541687.
[30] B.S. Arun, M.M. Gogoi, P. Hegde, A. Borgohain, S.K.R. Boreddy, S.S. Kundu, S.S. Babu, Carbonaceous aerosols over lachung in the eastern himalayas: primary sources and secondary formation of organic aerosols in a remote high-altitude environment, ACS Earth Space Chem. 5 (2021) 2493–2506, https://doi.org/10.1021/acsearthspacechem.1c00190.
[31] I. Marsli, M. Diouri, H. Steli, O. Salhi, Aerosol type influences on air and climate over the temperate areas, Air Qual. Atmos. Heal. (2022) 1557–1569, https://doi.org/10.1007/s11869-022-01203-1.
[32] P. Bernath, C. Boone, A. Pastorek, D. Cameron, M. Lecours, Satellite characterization of global stratospheric sulfate aerosols released by Tonga volcano, J. Quant. Spectrosc. Radiat. Transf. 299 (2023) 108520, https://doi.org/10.1016/j.jqsrt.2023.108520.
[33] T. Subba, M.M. Gogoi, K.K. Moorthy, P.K. Bhuyan, B. Pathak, A. Guha, M.K. Srivastava, B.M. Vyas, K. Singh, J. Krishnan, T.V. Lakshmi Kumar, S.S. Babu, New estimates of aerosol radiative effects over India from surface and satellite observations, Atmos. Res. 276 (2022) 106254, https://doi.org/10.1016/j.atmosres.2022.106254.
[34] V.-H. Peuch, R. Engelen, M. Rixen, D. Dee, J. Flemming, M. Suttie, M. Ades, A. Agustí-Panareda, C. Ananasso, E. Andersson, D. Armstrong, J. Barré, N. Bousserez, J.J. Dominguez, S. Garrigues, A. Inness, L. Jones, Z. Kipling, J. Letertre-Danczak, M. Parrington, M. Razinger, R. Ribas, S. Vermoote, X. Yang, A. Simmons, J.-N.T. Juan Garcés de Marcilla, The CAMS reanalysis of atmospheric composition, Atmos. Chem. Phys. 19 (2019) 3515–3556, https://doi.org/10.5194/acp-19-3515-2019.
[35] W.S. Huang, S.M. Griffith, Y.C. Lin, Y.C. Chen, C. Te Lee, C.C.K. Chou, M.T. Chuang, S.H. Wang, N.H. Lin, Satellite-based emission inventory adjustments improve simulations of long-range transport events, Aerosol Air Qual. Res. 21 (2021), https://doi.org/10.4209/AAQR.210121.
[36] L. Chutia, N. Ojha, I. Girach, B. Pathak, L.K. Sahu, C. Sarangi, J. Flemming, A. da Silva, P.K. Bhuyan, Trends in sulfur dioxide over the Indian subcontinent during 2003–2019, Atmos, Environ. Times 284 (2022) 119189, https://doi.org/10.1016/j.atmosenv.2022.119189.
[37] Y. Si, C. Yu, L. Zhang, W. Zhu, K. Cai, L. Cheng, L. Chen, S. Li, Assessment of satellite-estimated near-surface sulfate and nitrate concentrations and their precursor emissions over China from 2006 to 2014, Sci. Total Environ. 669 (2019) 362–376, https://doi.org/10.1016/j.scitotenv.2019.02.180.
[38] A. Bozzo, A. Benedetti, J. Flemming, Z. Kipling, S. Rémy, An aerosol climatology for global models based on the tropospheric aerosol scheme in the Integrated Forecasting System of ECMWF, Geosci. Model Dev. (GMD) 13 (2020) 1007–1034, https://doi.org/10.5194/gmd-13-1007-2020.
[39] S. Rémy, Z. Kipling, J. Flemming, O. Boucher, P. Nabat, M. Michou, A. Bozzo, M. Ades, V. Huijnen, A. Benedetti, R. Engelen, V.H. Peuch, J.J. Morcrette, Description and evaluation of the tropospheric aerosol scheme in the European centre for medium-range weather forecasts (ECMWF) integrated forecasting System (IFS-AER, cycle 45R1), Geosci, Model Dev 12 (2019) 4627–4659, https://doi.org/10.5194/gmd-12-4627-2019.
[40] DANE, Proyecciones nacionales y departamentales de Población 2005-2020, 1–300, https://www.dane.gov.co/files/investigaciones/poblacion/proyepobla06_20/7Proyecciones_poblacion.pdf, 2010.
[41] Gobernacion de La Guajira, Plan de desarrollo 2016 - 2019: Gobernación de La Guajira "Oportunidad para Todos y Propósito de País, Riohacha, 2016. http://www.laguajira.gov.co/web/attachments/article/3371/Plan.
[42] Cerrejón, Cerrejón cerró el 2016 con 32,4 millones de toneladas de carbón exportadas, Cifras Cerrejón, 2017, p. 2. http://www.cerrejon.com/site/sala-de-prensa/archivo-de-noticias/cerrejon-cerro-el-2016-con-32-4-millones-de-tonela.aspx. (Accessed 1 August 2017).
[43] R. Rojano, H. Arregoces, L.C. Angulo, G. Restrepo, Factor de analysis y cluster analysis para concentraciones de PM10 en minas de carbón a cielo abierto: cerrejón, Colombia, Interciencia 42 (2017) 44–50.
[44] EPA, Appendix J to Part 50-Reference Method for the Determination of Particulate Matter as PM10 in the Atmosphere, 1999. USA.
[45] EPA, Appendix B to Part 50, Reference Method for the Determination of Suspended Particulate Matter in the Atmosphere, high-volume method), USA, 2011.
[46] RTI, Standard Operating Procedure for PM2.5 Cation Analysis, 2009, pp. 1–11.
[47] RTI, Standard Operating Procedure for PM2.5 Anion Analysis, 2009, pp. 1–12.
[48] D.C. Carslaw, K. Ropkins, Openair - an r package for air quality data analysis, Environ. Model. Software (2012) 27–28, https://doi.org/10.1016/j.envsoft.2011.09.008, 52–61.
[49] R. Rojano, C.A. Manzano, R.A. Toro, R.G.E.S. Morales, G. Restrepo, M.A.G. Leiva, Potential local and regional impacts of particulate matter emitted from one of the world's largest open-pit coal mines, Air Qual. Atmos. Heal. 11 (2018) 601–610, https://doi.org/10.1007/s11869-017-0542-4.
[50] H.A. Arregocés, R. Rojano, L. Angulo, G. Restrepo, Intake fraction of PM 10 from coal mine emissions in the North of Colombia, J. Environ. Public Health (2018) 1–8, https://doi.org/10.1155/2018/8532463, 2018.
[51] MADS, Por la cual se adopta la norma de calidad del aire ambiente y se dictan otras disposiciones, MADS, Bogota D.C., Colombia, 2017. http://www.minambiente.gov.co.

[52] A. Hernadez, Análisis de la variación espacial de los componentes del material particulado respirable en la zona carbonífera del departamento del Cesar, Universidad Industrial de Santander, 2012.
[53] J. Kang, B.C. Cho, C.-B. Lee, Atmospheric transport of water-soluble ions (NO3(-), NH4(+) and nss-SO4(2-)) to the southern East Sea (Sea of Japan), Sci. Total Environ. 408 (2010) 2369–2377, https://doi.org/10.1016/j.scitotenv.2010.02.022.
[54] S.L. Mkoma, G.O. da Rocha, A.C.D. Regis, J.S.S. Domingos, J.V.S. Santos, S.J. de Andrade, L.S. Carvalho, J.B. de Andrade, Major ions in PM2.5 and PM10 released from buses: the use of diesel/biodiesel fuels under real conditions, Fuel 115 (2014) 109–117, https://doi.org/10.1016/j.fuel.2013.06.044.
[55] Z. Bozkurt, Seasonal variation of water-soluble inorganic ions in PM10 in a city of northwestern Turkey, Environ. Forensics 19 (2018) 1–13, https://doi.org/10.1080/15275922.2017.1408159.
[56] J. Watson, J. Chow, Chapter 20 - receptor models and measurements for identifying and quantifying air pollution sources, in: B.L. Murphy, R.D. Morrison (Eds.), Introd. To Environ. Forensics, third ed., third ed., Academic Press, San Diego, 2015, pp. 677–706.
[57] Z.L. Cheng, K.S. Lam, L.Y. Chan, T. Wang, K.K. Cheng, Chemical characteristics of aerosols at coastal station in Hong Kong. I. Seasonal variation of major ions, halogens and mineral dusts between 1995 and 1996, Atmos, Environ. Times 34 (2000) 2771–2783, https://doi.org/10.1016/S1352-2310(99)00343-X.
[58] Q. Yu, J. Chen, W. Qin, S. Cheng, Y. Zhang, M. Ahmad, W. Ouyang, Characteristics and secondary formation of water-soluble organic acids in PM 1 , PM 2.5 and PM 10 in Beijing during haze episodes, Sci. Total Environ. 669 (2019) 175–184, https://doi.org/10.1016/j.scitotenv.2019.03.131.
[59] J. Li, B. Chen, A.M.S. de la Campa, A. Alastuey, X. Querol, J.D. de la Rosa, 2005–2014 trends of PM10 source contributions in an industrialized area of southern Spain, Environ. Pollut. 236 (2018) 570–579, https://doi.org/10.1016/j.envpol.2018.01.101.
[60] J.S. Xu, J. He, S.N. Behera, H.H. Xu, D.S. Ji, C.J. Wang, H. Yu, H. Xiao, Y.J. Jiang, B. Qi, R.G. Du, Temporal and spatial variation in major ion chemistry and source identification of secondary inorganic aerosols in Northern Zhejiang Province, China, Chemosphere 179 (2017) 316–330, https://doi.org/10.1016/j.chemosphere.2017.03.119.
[61] J. Zhang, L. Tong, Z. Huang, H. Zhang, M. He, X. Dai, J. Zheng, H. Xiao, Seasonal variation and size distributions of water-soluble inorganic ions and carbonaceous aerosols at a coastal site in Ningbo, China, Sci. Total Environ. 639 (2018) 793–803, https://doi.org/10.1016/j.scitotenv.2018.05.183.
[62] L.M. Mcinnes, P.K. Quinn, D.S. Covert, T.L. Anderson, Gravimetric analysis, ionic composition, and associated water mass of the marine aerosol, Atmos. Environ. 30 (1996) 869–884, https://doi.org/10.1016/1352-2310(95)00354-1.
[63] Y. Cano, L.S. Castillo, B. Montilla, Determinación de iones solubles en partículas atmosféricas inhalables (PM10) por cromatografía iónica en Maracaibo, Venezuela, Rev. Bases La Cienc. 2 (2017) 1–16, https://doi.org/10.33936/rev.
[64] R. Rojano, H. Arregocés, E. Gámez Frías, Changes in ambient particulate matter during the COVID-19 and associations with biomass burning and Sahara dust in northern Colombia, Heliyon 7 (2021) e08595, https://doi.org/10.1016/j.heliyon.2021.e08595.
[65] W. You, Z. Zang, L. Zhang, Z. Li, D. Chen, G. Zhang, Estimating ground-level PM10 concentration in northwestern China using geographically weighted regression based on satellite AOD combined with CALIPSO and MODIS fire count, Remote Sens. Environ. 168 (2015) 276–285, https://doi.org/10.1016/j.rse.2015.07.020.
[66] M. Zeeshan, N.T. Kim Oanh, Assessment of the relationship between satellite AOD and ground PM10 measurement data considering synoptic meteorological patterns and Lidar data, Sci. Total Environ. (2014) 473–474, https://doi.org/10.1016/j.scitotenv.2013.12.058, 609–618.